



Phase Content and Flow Measurement of Bubble Flow based on New Experimental Pipeline

L. Fang^{1,2,3†}, S. Wang^{1,2,3}, S. Li^{1,2,3}, Y. Faraj^{4,5}, J. Tian^{1,2,3} and X. Li^{1,2,3†}

¹College of Quality and Technology Supervision, Hebei University, Baoding 071000, China

²Measuring Instruments and Systems Engineering Laboratory of Hebei Province, Baoding 071000, Hebei, China

³The Research Center of Industrial Metrology Engineering Technology of Baoding, Baoding 071000, Hebei, China

⁴Sichuan University, Chengdu 610000, Sichuan, China

⁵State Key Laboratory of Polymer Materials Engineering, Chengdu 610000, Sichuan, China

†Corresponding Author Email: fanslide@sina.com

(Received April 4, 2019; accepted July 9, 2019)

ABSTRACT

By combining near infrared spectroscopy and differential pressure meter to measure flow rate and phase volume fraction, a new structure of the near infrared system located in the position of the Venturi tube of long throat was proposed. The flow rate and volume fraction of the bubble flow were measured in a vertical experimental line. In terms of volumetric content measurement, based on typical flow characteristics, a void age model was established and experimentally verified. In terms of flow measurement, the classical measurement model is compared, and the uniform flow model is selected as the flow measurement model and corrected. The results show that the measurement error under the bubbly flow condition of the liquid volume fraction and the gas volume fraction was within $\pm 0.52\%$ and $\pm 10\%$, respectively. The relative error of total flow measurement was within $\pm 1.01\%$.

Keywords: Gas-liquid two-phase flow; Differential pressure flow meter; Volume fraction; Flow measurement.

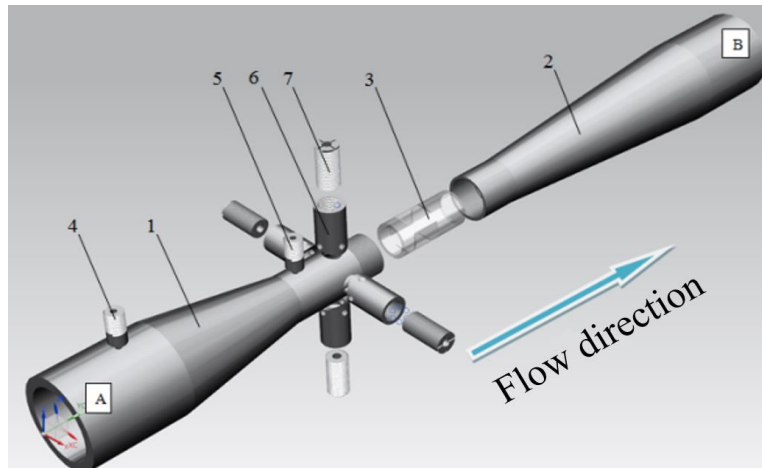
1. INTRODUCTION

Gas-liquid two-phase flow is encountered in a number of energy related industries such as petroleum, chemical industry, pipeline transportation, and nuclear reactors (Thandlam *et al.*, 2015; Shaban *et al.*, 2014). Obtaining the accurate measurement of gas-liquid two-phase flow mixture has become one of the challenges faced in the related industries. It is worth mentioning that phase Volume content and flow rate are two very important characteristic parameters of gas-liquid two-phase flow measurement (Yang *et al.*, 2018; Stahla *et al.*, 2004). Therefore, this work pay particular attention to the aforementioned two parameters.

Based on measurement principle, the method of flow measurement is usually categorized into four methods, namely differential pressure flow measurement method, velocity flow measurement method, volumetric flow measurement method, mass flow measurement method (Zheng *et al.*, 2018; Niu *et al.*, 2016). Differential pressure flow meters are the most widely used flow meters, particularly in

production line for measuring gas-liquid flow in industrial production. Orifice plates (Campos *et al.*, 2014), Venturi flow meters and V-cone flow meters are typical examples of differential pressure flow meters (Steven *et al.*, 2008). The void fraction detection technology and methods mainly include Quick Closing Valve, ray absorption method, electrical method and optical method (Ghassemi *et al.*, 2011; Zhao *et al.*, 2013, Pal *et al.*, 2018; Min, *et al.*, 2017; Yi *et al.*, 2018). Near-infrared light has been applied to the measurement of two-phase flow with achieving good results.

Lavallette *et al.* (2010) analyzed and measured volume fraction of solids and gas composition in gas-solid two-phase flow using spectral absorption method. Fang *et al.* (2018) proposed a method for measuring phase volume fraction of gas-liquid two-phase using near infrared absorption spectroscopy, in which real-time measurements were performed under stratified flow and bubble flow. Furthermore, Vendruscolo *et al.* (2014) developed a NIR optical tomography system for real-time monitoring of gas-liquid two-phase flow. Sajid *et al.* (2008)



(1-Shrink tube, 2-divergent tube, 3-Quartz transparent tube, 4、5-Pressure taps, 6-near-infrared probe fixing pipe, 7-pressing bolt)

Fig. 1. Structure of the new measuring device.

investigated the steady flow of third grade fluid past a horizontal porous flat plate with partial slip. They solved the arising non-linear problem numerically using a finite element method. Ullmann *et al.* (2000) investigated the counter current flow in a vertical, off vertical and inclined columns. The two phase fluid is also important in studying the blood flow particularly for the Fahraeus-Lindqvist (F-L) effect. Majhi and Usha (1988) investigated the F-L effect by considering blood as a third grade non-Newtonian fluid. Pouriya *et al.* (2017) proposed a method of calculating the speed of sound and suggested a new practical equation, in which it is correlated with fluid properties, and was developed by genetic Algorithm.

In order to be able to measure the phase content and flow rate of an accurate two-phase flow using near-infrared technology, this paper proposes a new device. The device arranges a new structure that places the near-infrared measurement system on the throat section of the venturi, in which the optical path is reduced as a result of shrinking the flow cross-sectional domain. Thus, the distance between the near-infrared transmitting probe and the receiving probe is reduced, which results in the improvement of the received signal and keeping the signal characteristics of the flow pattern unchanged, hence the unnecessary energy loss is reduced. Finally, the two parameter measurement of phase Volume content and differential pressure information is achieved, and a new phase Volume content and flow measurement model is established.

2. OPTIMIZATION DESIGN OF NEW MEASURING DEVICE

The new measuring device makes use of Venturi as the basic structure. In order to accommodate the near-infrared measurement system, the length of the Venturi tube (throat section) is extended, on which the near-infrared measurement system is mounted. By combining near-infrared measurement system

with venturi the two important flow parameters can be obtained: the phase ration, which is measured by the near-infrared system and the flow rate, which is measured by the differential pressure method of the venturi. The schematic diagram of the novel structured device is shown in Fig. 1. The overall structure of the device is a long cylindrical throat venturi tube, including conical convergent section 1, conical divergent section 2, a transparent pipe section 3 embedded therein, upstream and downstream pressure taps 4, 5 respectively, a near-infrared probe fixing pipe 6, and a pressing bolt 7.

It is worth pointing out that the main structure of the long-throat neck Venturi is a non-standard throttling device, the main function of which is to generate a differential pressure value as the fluid flows through the section. Using CFD software for simulation, the pressure cloud map, velocity cloud map and velocity vector map were obtained. Figure 2 only shows the velocity cloud map. The flow state of the fluid in the structure of different size parameters under the same simulation condition is observed, and the structure with a larger effective differential pressure value and less pressure loss ratio is selected to determine the main size of the device. Finally, the processing map of the device is drawn to fabricate the prototype measuring device, as shown in Fig. 5.

3. EXPERIMENTAL TEST

A mixture of air and water was used in the two-phase flow experiments. The night road standard table is Endress+Hauser DN10 and DN40 diameter electromagnetic flow meter with a measurement accuracy of 0.15%. The gas path uses Alicat's MC series mass flow measurement controller with a range of 0-10Slpm/min and an accuracy of 0.2% of full scale, and the wavelength of the beam of selected near-infrared measurement is 980 nm.

In order to cover the desired gas-liquid two-phase flow pattern, 35 operating points were set, covering

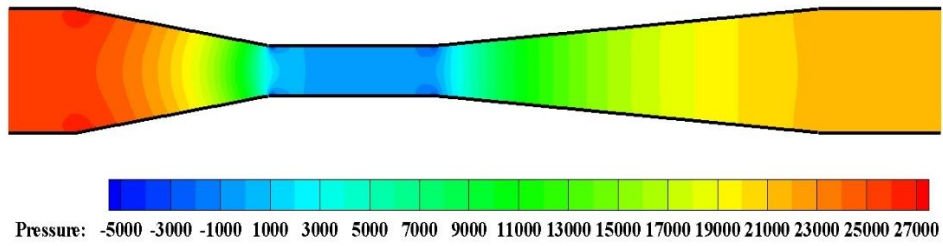


Fig. 2. Pressure field of the symmetrical plane.

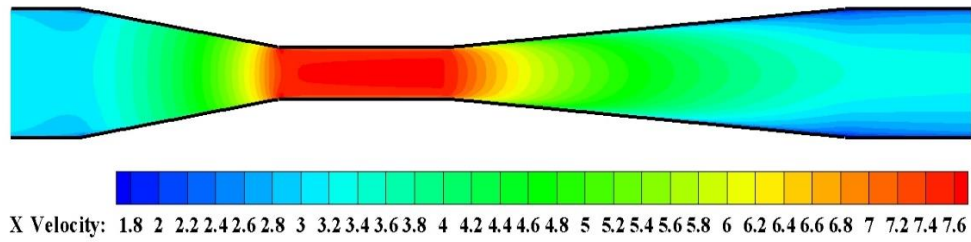


Fig. 3. Velocity field of the symmetrical plane.

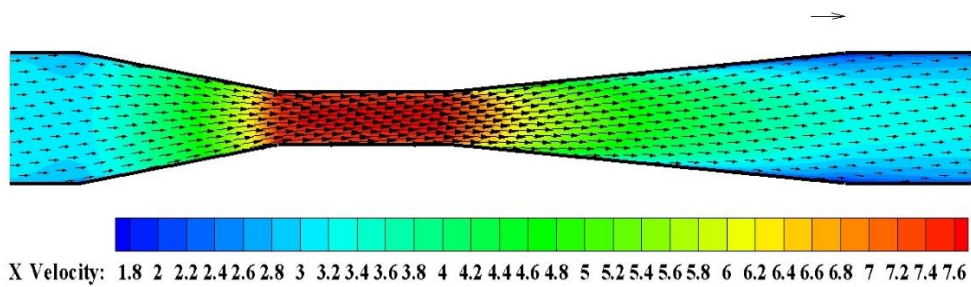


Fig. 4. Velocity vector diagram of the symmetrical planes.

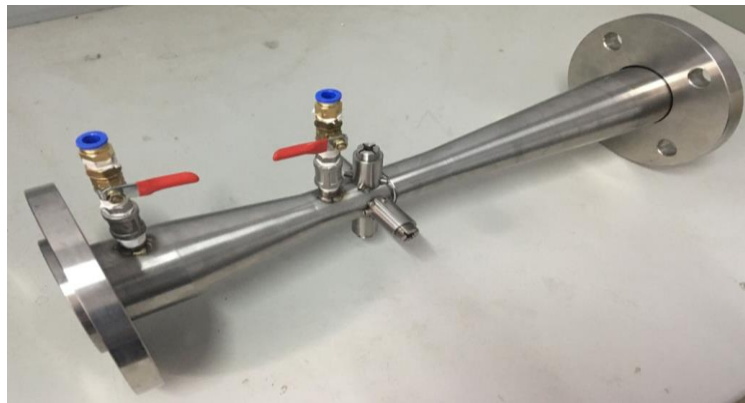


Fig. 5. Prototype of the measuring device.

the water flow range of 8-11 m³/h and the gas flow range was 0.12-0.6 m³/h. Three replicate experiments were performed to obtain 105 sets of experimental data.

Establishment of Phase Volume Content Measurement Model

The liquid phase volumes fraction at each operating

point is obtained by Eq. (1), which is considered as the actual value of the liquid phase volume fraction:

$$\beta_l = \frac{Q_l}{Q_l + \frac{(101.3 + P_g) \times Q_g \times (273.2 + T_b)}{(273.2 + T_g) \times (101.3 + P_b)}} \quad (1)$$

Where Q_l , Q_g are volume flow rate of liquid phase

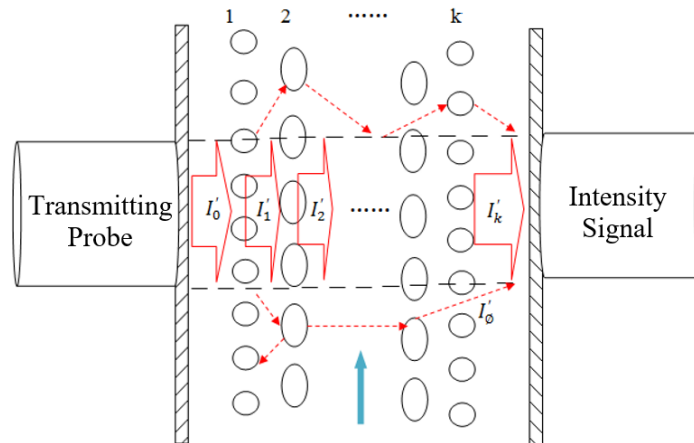


Fig. 6. Schematic diagram of detecting light beam.

and gas phase, respectively (m^3/h); P_g is gas pressure (KPa); T_g is gas temperature ($^{\circ}C$); P_b is the Pressure gauge pressure of experimental tube (KPa); T_b is background temperature of experimental tube ($^{\circ}C$).

Near-infrared light refers to light having a wavelength between 780 nm and 2500 nm between visible light and mid-infrared light. The principle of measuring the phase Volume content ratio of near-infrared light is based on the Lambert-Beer absorption law and the law of superposition of absorbance characteristics.

A beam of monochromatic parallel light illuminates a uniform light-absorbing medium, for which the relationship can be expressed by Lambert-Beer law as Eq. (2):

$$I = I_0 e^{-\alpha_{\Delta}(\lambda)d} \quad (2)$$

Where I_0 and I are incident light intensity and light intensity (candela), respectively; d is media thicknesses (cm); $\alpha_{\Delta}(\lambda)$ is the absorption coefficient of light with wavelength of λ for material Δ (cm^{-1}).

For near-infrared light of a particular wavelength, the absorbance of the solution is equal to the linear sum of the absorbance of the components with absorption. The equation for the linear superposition law of absorbance is given by Eq. (3):

$$A = \sum_{i=1}^n A_i \quad (3)$$

Based on Lambert-Beer's law and the law of linear superposition of absorbance, Eq. (4) is obtained.

$$\frac{I_i}{I_0} = e^{-\alpha_i b_i} \quad (4)$$

Where α_i is absorption coefficient of near-infrared

light used for water; b_i is the depth of the liquid layer in the optical path; I_i is the light intensity when the depth of the liquid layer is b_i .

The liquid thickness C_i of the transition layer and the turbulent core region can be expressed by Eq. (6).

$$c_i = b_i \times \beta_l \quad (5)$$

Where β_l is the liquid phase volume fraction, h is the propagation distance of the light beam in the flowing two-phase flow medium:

By combining Eqs. (4) and (5) (6) is obtained.

$$\frac{I_i}{I_0} = e^{-\alpha_l (b_i \times \beta_l)} \quad (6)$$

4. MODEL ESTABLISHMENT

For the sake of simplicity, the prevalent flow pattern (bubble flow) is taken as a homogeneous flow model. The gas-liquid two-phase mixture is regarded as a homogeneous medium with no slip velocity, and the flow parameters are taken as the average of the corresponding parameters of the two phases. Based on this model, bubble flow is treated as a single-phase flow with average fluid characteristics. In addition, the gas bubbles are assumed to have spherical shape, which are uniformly distributed within the liquid phase across the pipe cross-section.

The schematic diagram of detecting light beam affected by two-phase interface of bubble flow is shown in Fig. 6. Irrespective of the effect of light absorption in gas and liquid phases, the attenuation effect of the beam's refraction and reflection on the transmitted optical signal is analyzed separately. The attenuation effect of refraction and reflection of the beam at gas-liquid interface is analyzed. When the near-infrared detection light beam with the incident optical intensity I'_0 is irradiated to the first layer of gas bubbles, refraction and reflection occur at the

Table 1 Undetermined coefficients of fitting

Liquid flow (m ³ /h)	A	B	K	L
8	5863.6998	-1212.6917	2.2790	84.0110
8.5	18688.0881	-2944.9174	1.8392	84.3342
9	17877.7072	-2428.1120	1.7599	84.8885
9.5	207339.7000	-22880.1643	1.7826	80.1685
10	1224110.0000	-84692.7458	1.9639	74.3836
10.5	1665460.0000	-72189.1673	2.1387	71.3598
11	1142320.0000	-2565.2183	2.4438	68.0028
The average	611665.5993	-26987.5738	2.0296	78.1640
Variation coefficient	1.0192	-1.1913	0.0928	0.0652

gas-liquid interface, which leads to the attenuation of the intensity of light passing through the light path to I_1' , the attenuation coefficient is a_1 , and can be expressed as $I_1' = a_1 \times I_0'$. In the simplified homogeneous flow model, the air bubbles are evenly distributed, thus a_1 is a continuous periodic function on time t : $a_1 = f(t)$, where $f(t)$ is a continuous function with a period of T . According to the mean value theorem of integrals and the definite integral characteristic of periodic function, when the measurement time interval $[t_1, t_2]$ is sufficiently larger than the period T , the following can be obtained:

$$\frac{\int_{t_1}^{t_2} f(t) dt}{t_2 - t_1} \approx \frac{\int_{t_1}^{t_1 + nT} f(t) dt}{(t_1 + nT) - t_1} \quad (7)$$

$$= \frac{n \int_{t_1}^{t_1 + T} f(t) dt}{nT} = \frac{\int_0^T f(t) dt}{T} = A_1$$

The above correlation implies that the average value of the attenuation coefficient a_1 of the first layer of bubbles on the light is approximately equal to a fixed value A_1 within the measurement time interval $[t_1, t_2]$. Therefore, in the measurement time interval, the average value of the intensity of the near-infrared detection beam, after the first layer of bubbles is attenuated, is a fixed value, which can be expressed as:

$$\overline{I_1'} = A_1 \times I_0' \quad (8)$$

Similarly, the average value of the attenuation coefficient $a_2, a_3, a_4 \dots$ of the 2, 3, 4...k layer of bubbles on the light is approximately equal to a fixed value $A_2, A_3, A_4 \dots A_k$ within the measurement time interval $[t_1, t_2]$. When near-infrared detection beam attenuation passes through the k layer of the bubble, the average value of the light intensity $\overline{I_k'}$ can be expressed as:

$$\overline{I_k'} = A_k \times \overline{I_{k-1}'} = \dots = A_1 A_2 A_3 \dots A_k \times I_0' \quad (9)$$

In addition, after some light is reflected multiple times, the light returns to the optical path and enters the optical path. This part of the light is recorded as I_ϕ' . Therefore, the average value of the light intensity signal $\overline{I_r'}$ received by the near-infrared receiving probe can be expressed as:

$$\overline{I_r'} = \overline{I_k'} + \overline{I_\phi'} = A_1 A_2 A_3 \dots A_k \times I_0' + \overline{I_\phi'} \quad (10)$$

In summary, when the near-infrared light beam with constant incident light intensity passes through the bubbly flow medium, it is affected by the absorption of the liquid phase and the refraction and reflection of the two-phase interface, resulting in the attenuation of the received light intensity at the receiving probe. Combining Eqs. (6) and (10), Eqs. (11) and (12) can be obtained:

$$\frac{(\overline{I_n'} - \overline{I_\phi'}) / (A_1 A_2 A_3 \dots A_k)}{\overline{I_{r0}'}} = e^{-\alpha_1 (b_1 \times \beta_1)} \quad (11)$$

Where $\overline{I_n'}$ is the average value of light intensity by the receiving is probe under bubble flow condition; $\overline{I_{r0}'}$ is the average light intensity of the receiving probe in empty state.

The relationship between the liquid volume fraction under bubble flow condition and the received light intensity signal of the near-infrared system can be obtained. The fitting model of the liquid volume content measurement is:

$$y = K \times \ln(A \times x + B) + L \quad (12)$$

Where y is volume fraction of the liquid phase; x is the ratio of the mean value of light intensity signal under bubble flow condition to the average value of the received by the near-infrared probe under the empty condition, A, B, K, L are the undetermined coefficient, the value of which are shown in Table 1.

Bring the values of $A, B, K,$ and L calculated in Table 1 into Eq. (12) to gets:

$$y = 2.0296 \times \ln(A \times x + B) + 78.1640 \quad (13)$$

Figure 7 shows the the relationship between undetermined coefficients *A* and *B* and the liquid flow rate.

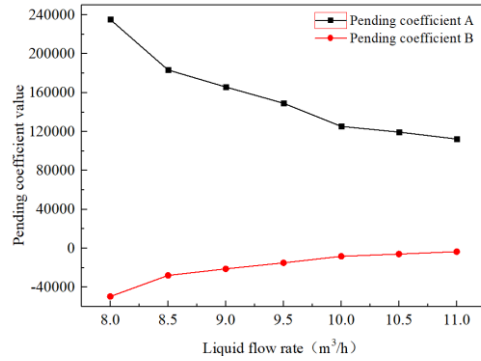


Fig. 7. Relation between the undetermined.

Coefficients A, B and Liquid flow Rate

By observing (Fig. 7), it can be seen that the relationship of the undetermined coefficients *A* and *B* is an exponential as a function of liquid flow rate. The fitting results are shown in Fig. 8 and Fig. 9.

$$y = e^{a+bx} + c \quad (14)$$

$$y = -e^{a+bx} + c \quad (15)$$

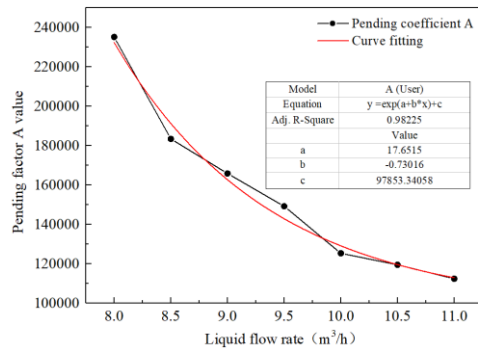


Fig. 8. Fitting result of the undetermined Coefficients A and liquid flow rate.

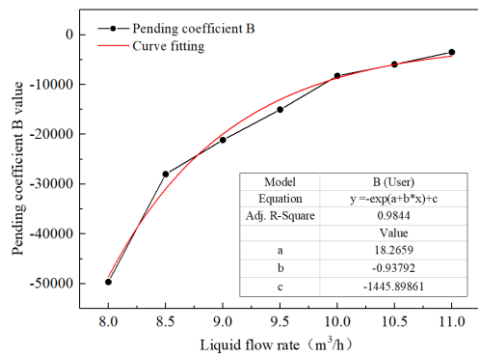


Fig. 9. Fitting result of the undetermined Coefficients B and liquid flow rate.

The coefficient of determination R^2 of the two fitting results are above 0.98. The undetermined coefficients *A* and *B* as a function of the liquid flow rate are given in Eq. (19) and Eq. (20) respectively. The liquid volume content model can be described by Eq. (21):

$$A = e^{17.6515-0.7302Q_l} + 97853.3406 \quad (16)$$

$$B = -e^{18.2659-0.9379Q_l} - 1445.8986 \quad (17)$$

Bring the above formulas (16) and (17) into the formula (15):

$$\beta_l = 2.0296 \ln \left(\frac{\left(e^{17.6515-0.7302Q_l} + 97853.3406 \right)^x}{\left(-e^{18.2659-0.9379Q_l} - 1445.8986 \right)} \right) + 78.1640 \quad (18)$$

The second experimental data was used as verification data, to examine the effect of phase Volume content measured by the new device and the new model. The actual value of the gas phase volume fraction and the measured value of the gas phase volume fraction can be obtained by Eq. (18) and Eq. (19):

$$\beta_g = (1 - \beta_l) \times 100\% \quad (19)$$

Using the new device and the new measurement model, the relative error distribution of the liquid volume fraction and the measured gas volume fraction was experimentally shown in Figs. 10 and 11. The relative error of the liquid volume fraction is within $\pm 0.52\%$, and the relative error of the gas phase volume fraction is within $\pm 10\%$.

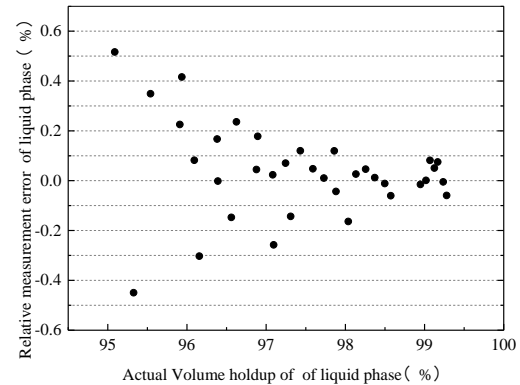


Fig. 10. Relative error distribution of the Liquid Volume content.

5. THEORETICAL ANALYSIS OF FLOW MEASUREMENT

A variety of measurement models through experiments have been obtained by a number of researchers. For example, homogeneous flow model, James model, Separated flow model, Murdock mode, Chisholm model, Smith & Leang model, Lin Zonghu model and so on. In this paper, the bubble

flow is treated as a homogeneous flow model, and the gas and liquid phases are in a thermodynamic equilibrium state. In other words, the two phases have the same temperature and are all in a saturated state. The flow rates of the gas and liquid phases are equal. Therefore, the bubble flow is measured with the reference to the homogeneous flow model and the James model.

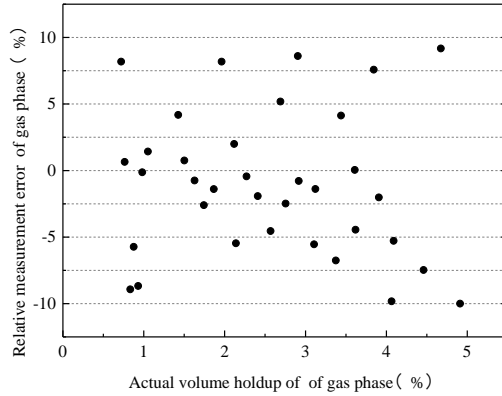


Fig. 11. Relative error distribution of the gas phase Volume content.

1) Homogeneous flow model

There is no slip velocity between the gas phase and liquid phase in homogeneous flow model. The two-phase mixing density is shown in Eq. (20):

$$\frac{1}{\rho_w} = \frac{x}{\rho_g} + \frac{1-x}{\rho_l} \tag{20}$$

$$x = \frac{(1-\beta_l)\rho_g}{(1-\beta_l)\rho_g + \beta_l\rho_l} \tag{21}$$

Where ρ_w is the mixture density of gas-liquid two-phase flow (kg/m^3); ρ_g, ρ_l are densities of gas phase and liquid phase, respectively; x is the volume fraction. If the gas-liquid two-phase flow is treated as a single-phase flow with density ρ_w , the total volume flow can be obtained by Eq. (22):

$$Q_w = \frac{C\epsilon\beta^2\pi R^2}{\sqrt{1-\beta^4}} \sqrt{\frac{2\Delta P_w \rho_g}{\rho_l + x^{1.5} \times \left(1 - \frac{\rho_g}{\rho_l}\right)}} / \rho_w \tag{22}$$

Where Q_w is the total volume flow of the two-phase flow (m^3/s); C is the discharge coefficient; ϵ is the expansion coefficient; β is the throttle ratio of the throttle set; R is the radius of inlet pipe; ΔP_w is differential pressure produced by the mixed gas-liquid two-phase flow through the throttling set (Pa).

2) James model (James, 1968)

Through a large number of experiments, James has found that the accuracy of the homogeneous flow model can effectively improve the measurement by using effective volume fraction x_m instead of true volume fraction x in homogeneous flow model.

$$x_m = x^{1.5} \tag{23}$$

Equation (23) shows the flow calculation formula of James model:

$$Q_w = \frac{C\epsilon\beta^2\pi R^2}{\sqrt{1-\beta^4}} \sqrt{\frac{2\Delta P_w \rho_g}{\rho_l + x^{1.5} \times \left(1 - \frac{\rho_g}{\rho_l}\right)}} / \rho_w \tag{24}$$

The temperature, pressure and flow meter measured data in the experiment are placed in Eq. (25), and the calculated result is used as the actual total volume flow of the gas-liquid two-phase flow at the experimental section.

$$Q_w = Q_l + \frac{(101.3 + P_g) \times Q_g \times (273.2 + T_b)}{(273.2 + T_g) \times (101.3 + P_b)} \tag{25}$$

Figure 12 shows the relationship between the total volumetric flow of the gas-liquid two phase and the differential pressure measured by the differential pressure transmitter.

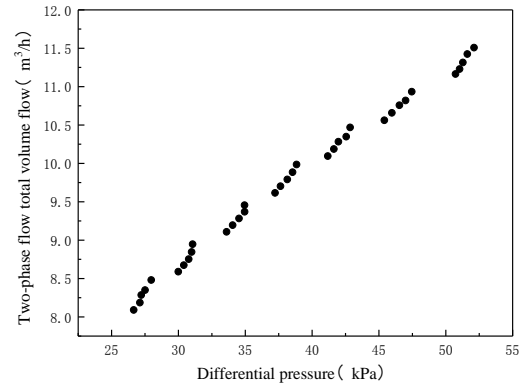


Fig. 12. Relationship diagram of the differential pressure and the total volume flows.

The measured density of gas phase in the pipe is determined by Eq. (26):

$$\rho_g = \frac{(101.3 + P_b) \times \rho_0 \times 273.2}{(273.2 + T_b) \times 101.3} \tag{26}$$

Where ρ_0 is the gas density under standard conditions ($\rho_0 = 1.29 \text{ kg/m}^3$).

Two-phase mixture density ρ_w , the real volume fraction x and the effective volume fraction x_m can be calculated by Eqs. (20), (21) and (23).

For a throttle set with a known throttle ratio, ϵ only depends on the upstream pressure, differential pressure, and isentropic exponent of the throttling device, and it can be determined using Eq. (27):

$$\epsilon = \sqrt{\frac{\frac{2}{\kappa\tau\kappa}}{\kappa-1} \left(\frac{1-\beta^4}{1-\beta^4\tau\kappa} \right) \left(\frac{\frac{\kappa-1}{1-\tau\kappa}}{1-\tau} \right)} \tag{27}$$

$$\tau = \frac{101.3 + P_b - \Delta P_w}{101.3 + P_b} \quad (28)$$

Where τ is the pressure ratio, κ is the isentropic exponent. The isentropic exponent is the ratio of the relative change in pressure to the density in the process of isentropic (reversible adiabatic). This work takes $\kappa=1.4$.

Each value is put into the flow formula of the homogeneous flow model and the volume flow rate $Q_{w(J)}$ is obtained, then the measured values and the actual values are compared, from which the relative error of the measurement is calculated.

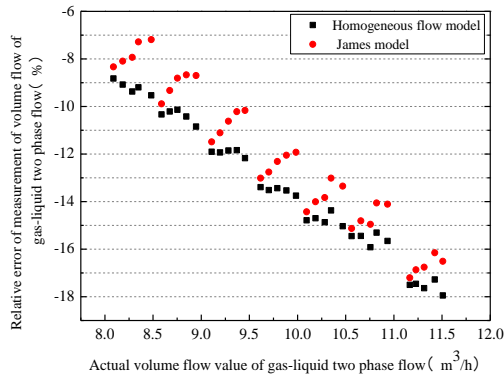


Fig. 13. Distribution diagram of relative measurement error of classical model.

Figure 13 shows that the relative error of the gas-liquid two-phase flow volume flow calculated by the uniform flow model is between -17.95% and -8.82%. The relative error of the volumetric flow of the gas-liquid two-phase flow calculated by the James model is between -17.21% and -7.19%. Although the measured relative error of the James model is smaller than the measured relative error of the homogeneous flow model. However, as shown in fig. 14, the relationship between the flow measurement value calculated by the homogeneous flow model and the true flow value is linear. Therefore, the final measurement model is selected as the homogeneous flow model, and the correction factors k and l are introduced on the basis of the homogeneous flow model. The flow measurement model is:

$$Q_w' = k \times Q_{w(J)} + l = k \times \frac{C \varepsilon \beta^2 \pi R^2}{\sqrt{1 - \beta^4}} \sqrt{\frac{2 \Delta P_w \rho_g}{\rho_l + x \times \left(1 - \frac{\rho_g}{\rho_l}\right)}} / \rho_w + l \quad (29)$$

The correction factor is obtained by fitting the actual volume of the total volume flow of the two phase flow with the flow rate measured by the homogeneous flow model, and the result is shown in the Fig. 14.

Where the coefficient of determination R^2 is 0.97, correction factors k, l are 1.65 and -4.14 respectively.

The second experimental data is used as verification data to test the effect of measuring the total volume flow of the two-phase flow by using the new device

and final measurement model. The relative error results are shown in Fig. 15.

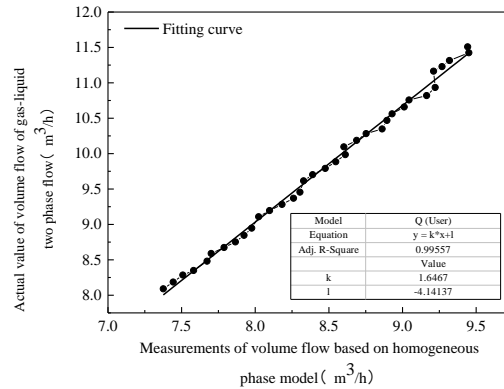


Fig. 14. Fitting relationship between flows measured values and actual values based on homogeneous flow model.

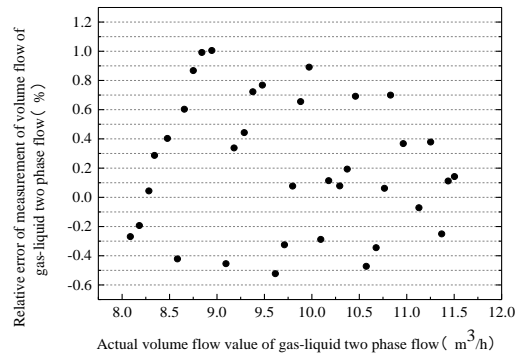


Fig. 15. Distribution of relative Measurement error.

As shown in Fig. 16, the relative error of gas-liquid two-phase flow volume flow measurement is within $\pm 1.01\%$.

Error analysis: 1. The measurement result of the near-infrared light being reflected to the volume fraction brings errors. 2. The pressure loss of the experimental pipeline brings errors to the measurement results of the differential pressure transmitter.

Repeatability of the experiment: The experiment was performed by the same operator from the same laboratory in the same laboratory. Three replicate experiments were performed on the same subject in the short term. The standard deviation of near-infrared and differential pressure data was calculated using Bessel's formula under repeated conditions. By calculating the standard deviation of different operating points, finding the maximum standard deviation is the repeatability of the measurement results. The standard deviation of the near-infrared measurement is 0.045, and the standard deviation of the differential pressure measurement is 0.029.

6. CONCLUSION

In order to optimize the system structure and closely

Table 2 Standard error table

Near-infrared liquid phase point standard deviation						
8 m ³ /h	8.5 m ³ /h	9 m ³ /h	9.5 m ³ /h	10 m ³ /h	10.5 m ³ /h	11 m ³ /h
0.024	0.042	0.045	0.042	0.04	0.043	0.042
Differential pressure liquid phase point standard deviation						
8 m ³ /h	8.5 m ³ /h	9 m ³ /h	9.5 m ³ /h	10 m ³ /h	10.5 m ³ /h	11 m ³ /h
0.027	0.027	0.022	0.024	0.029	0.028	0.028

combine the infrared information and differential pressure information, a new structure is designed to arrange the near-infrared system at the throat of the Long throat Venturi tube.

Based on the basic equations of gas-liquid two phase flow and the definition of flow parameters, a theoretical model for the new phase Volume content and volume flow of bubble flow is developed. The dual-parameter measurement effect of differential pressure measurement flow rate and near-infrared measurement phase hold rate is achieved.

ACKNOWLEDGEMENTS

The authors gratefully acknowledge the support of Hebei University (hbu2018ss81), the National Natural Science Foundation of China (G61475041), Natural Science Foundation of Hebei Province (E2017201142) and Subtask National Key Research Task Plan (2016YFF0203103-3, 2017YFC0805703).

REFERENCES

- Campos, S. R. V, J. L. Baliño, I. Slobodcicov, D. F. Filho, and E. F. Paz (2014). Orifice plate meter field performance: Formulation and validation in multiphase flow conditions. *Experimental Thermal & Fluid Science* 58, 93-104.
- Fang, L. D., Y. J. Liang, Y. J. Zhang, C. Zhang and J. Z. Gao (2014). The study of flow characteristic of gas-liquid two-phase flow based on the near-infrared detection device. *AIP Conference Proceedings*, 1592, 2014, pp. 236-245.
- Ghassemi, H. and H. F. Fasih (2011). Application of small size cavitating venturi as flow controller and flow meter. *Flow Measurement and Instrumentation* 22(5), 406-412.
- Lavallette, J. P., G. S. Patience and J. Chaouki (2010). Simultaneous quantitative measurement of gaseous species composition and solids volume fraction in a gas/solid flow. *Aiche Journal* 56(11), 2850-2859.
- Majhi, S. N. and L. Usha (1988). Modelling the Fahraeus-Lindqvist effect through fluids of differential type. *International Journal of Engineering Science* 26, 503-508.
- Min, S. K., A. L. Bo, W. Y. Woo, Y. G. Lee, W.J. Dong S. Kim (2015). An improved electrical-conductance sensor for void-fraction measurement in a horizontal pipe. *Nuclear Engineering and Technology* 47(7), 804-813.
- Niu, Z., Q. Zhao and X. Feng (2016). Numerical simulation and optimization of ring groove flow meter. *China Measurement & Test* 42, 122-126.
- Pal, A. and B. Vasuki (2018). Void fraction measurement using concave capacitor based sensor-Analytical and experimental evaluation. *Measurement* 124, 81-90.
- Pouriya H., Niknam, Daniele Fiaschi, H. R. *et al.*, (2017). An improved formulation for speed of sound in two-phase systems and development of 1D model for supersonic nozzle. *Fluid Phase Equilibria* 446, 18-27
- Sajid, M, R. Mahmood and T. Hayat (2008). Finite element solution for flow of a third grade fluid past a horizontal porous plate with partial slip. *Computers & Mathematics with Applications* 56, 1236-1244.
- Shaban, H. and S. Tavoularis (2014). Identification of flow regime in vertical upward air-water pipe flow using differential pressure signals and elastic maps. *International Journal of Multiphase Flow* 61(5), 62-72.
- Stahla, P. and P. R. v. Rohr (2004). On the accuracy of void fraction measurements by single-beam gamma-densitometry for gas-liquid two-phase flows in pipes. *Experimental Thermal and Fluid Science* 28(6), 533-544.
- Steven, R. (2008). A dimensional analysis of two phase flow through a horizontally installed Venturi flow meter. *Flow Measurement and Instrumentation* 19(6), 342-349.
- Thandlam, A. K., T. K. Mandal and S. K. Majumder (2015). Flow pattern transition, frictional pressure drop, and holdup of gas non-Newtonian fluid flow in helical tube. *Asia-Pacific Journal of Chemical Engineering* 10, (3), 422-437.
- Ullmann, A., M. Zamir, L. Ludmer and N. Brauner (2000). Characteristics of liquid-liquid

- counter current flow in inclined tubes— Application to PTE process. *Proceedings of the International Symposium on Multi- phase flow and Transport Phenomenon, Anatalya, Turkey Int Comm Heat Mass Transf.* 112–116.
- Vendruscolo, T. P., M. V. W. Zibetti, R. L. Patyk, G. Dutra, R. E. M. Morales and C. Martelli (2014). Development of NIR optical tomography system for the investigation of two-phase flows. *Instrumentation and Measurement Technology Conference. IEEE*, 2, Montevideo (UY), 1576-1579.
- Yang, Y., D. Wang, P. Niu, M. Liu and S. Wang (2018). Gas-liquid two-phase flow measurements by the electromagnetic flow meter combined with a phase-isolation method. *Flow Measurement and Instrumentation* 60, 78-87.
- Yi, M., T. Qiu, M. Okubo, X. Li and L. Guo (2018). Innovative on-line near-infrared (NIR) spectroscopy to estimate content of each phase in composite polymer particles prepared by seeded emulsion polymerization. *Vibrational Spectroscopy* 95, 23-31.
- Zhao, Y., Q. Bi and R. Hu (2013). Recognition and measurement in the flow pattern and void fraction of gas-liquid two-phase flow in vertical upward pipes using the gamma densitometer. *Applied Thermal Engineering* 60, (1-2), 398-410.
- Zheng, X., X. Sun and B. Bai (2018). Flow rate measurement of low GVF gas-liquid two-phase flow with a V-Cone meter. *Experimental Thermal and Fluid Science* 91, 175-183.